



Comparison of the structure in human skin and acquired cholesteatoma

Bachelor (BSc) thesis from the Department of Biochemistry and Molecular Biology, University of Southern Denmark

Marie Karen Tracy Hong Lin

31-08-2015

Supervisor: Jonathan Brewer

Table of Contents

Introduction.....	3
Theory and background.....	4
The human epidermis.....	4
Cholesteatoma	9
Material and method.....	11
Freezing of sample.....	11
Slicing of tissue samples	11
Labeling with TopFluor dye	12
Indirect immunocytochemistry	12
Confocal fluorescence microscopy.....	13
STED microscopy	13
CARS microscopy	14
Results	15
Discussion	25
Conclusion	28
Reference	28
Attachment.....	30

Abstract

I denne projekt sammenlignes væv fra øresygdommen kolesteatom med stratum corneum fra menneskehud. Proteinerne cytokeratin-1, filaggrin og desmoglein-1 blev farvet ved hjælp af antistoffer og blev visualiseret ved hjælp af forskellige metoder, såsom confocal lasermikroskopi, superresolution STED (Stimulated emission depletion) mikroskopi og CARS (Coherent anti-Stokes Raman Scattering) mikroskopi. Filaggrin blev fundet i kolesteatomet, hvilket tyder på at kolesteatomet ligner den nedre zone af stratum corneum i hud. Dog i en meget fortykket udgave.

Størrelsen af korneocytter i kolesteatomerne og hud blev målet. Korneocytterne i kolesteatomerne var ca. to gange så høj som dem i hud, hvilket tyder på at de ikke var fuldmoden. Resultaterne fra antibody farvning tydet på en defekt barrieren funktion i kolesteatomet. Dette sammen med de umodne korneocytter og den fortykket stratum corneum kunne tyde på at en defekt barrier i kolesteatomet medføre den øget epidermal proliferatiom som findes i kolesteatomet.

Introduction

Acquired cholesteatoma is a destructive and expanding growth consisting of keratinizing squamous epithelium in the middle ear. It originates from the adjoining epidermis in several ways, but the exact causation is presently still unknown. Cholesteatoma is believed to be genetic in some individuals and associated to chromosomal imbalances. At present the only treatment for cholesteatoma is operation. Many complications can arise from cholesteatoma in patients and a better understanding of the disease could be informative to enhance the development of drugs against the disease. Statistics showed that the disease is most common among male individuals and undeveloped countries have a high total number of cholesteatoma cases. Cholesteatoma in Scandinavia has been found to be approximately 3 per 100 000 children and 9.2 per 100 000 Caucasian adults (1). Cholesteatoma is still an ongoing case studied by scientist and little is known about the exact molecular mechanisms of cholesteatoma. In a study done by Bloksgaard et al. 2012 (2), lipid composition and extracellular membranes analysis demonstrate that the cholesteatoma resembles the stratum corneum of the human skin. It is therefore of interest to further study the resemblance of the cholesteatoma to the skin stratum corneum. In particular it is interesting to investigate some of the important proteins present in the stratum corneum. The proteins chosen to be investigated in this project are the cytokeratin 1, filaggrin and desmoglein1. Images of the lipids are also taken both by labeling with the lipophilic dye TopFluor and by CARS microscopy. The proteins on the other hand are labeled by the process known as indirect immunocytochemistry and imaged using confocal fluorescence microscopy, superresolution STED microscopy together with CARS microscopy.

In this study, part of the focus is on the permeability barrier properties of the cholesteatoma. Bloksgaard et al. 2012 (2) demonstrates that the cholesteatoma resembles very thick stratum corneum and Proksch et al. 1991 (3) showed that defect permeability properties in the skin is related to increased epidermal proliferation. In this study, we use filaggrin as a marker protein to make sure that the cholesteatoma resembles the stratum corneum. Filaggrin is known from literature to only be synthesized in the stratum corneum. The visible similarity in structures between the cholesteatoma and the skin stratum corneum will be used to provide information about the organization, structure and barrier function of the cholesteatoma.

Theory and background

The human epidermis

The human epidermis is a very important component of the body because it acts as a protective barrier against entry of microorganisms, blocks radiation and prevent water loss from an individual. The epidermis mainly consists of four layers which are the Stratum Basale (SB), Stratum Spinosum (SS), Stratum Granulosum (SG) and Stratum Corneum (SC). The different layers are also known as basal, spinous, granular and cornified layer which are simplified names for stratum basale, stratum spinosum, stratum granulosum and stratum corneum respectively. An illustration of the epidermis layers is shown in figure 1. The main cell type present in the epidermis is keratinocyte and it is made up of 90% of the keratinocyte cells (4).

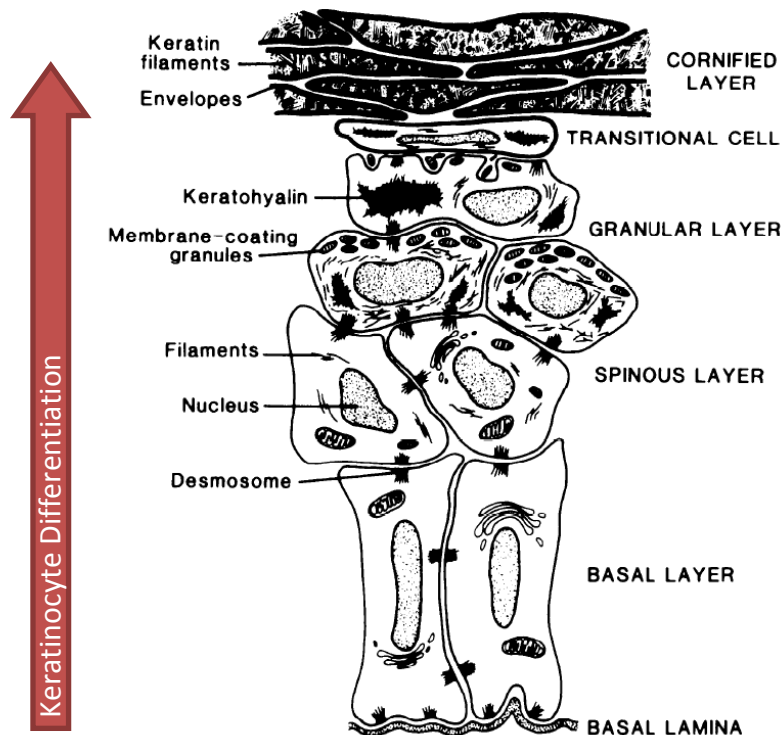


Figure 1 illustrates the structure changes of the keratinocyte cells during the differentiation process in the epidermis section of the skin. The red arrow indicates the direction of the keratinocyte differentiation which starts from the basal layer to the cornified layer (Eckert R. L. 1989).

The basal lamina as illustrated in figure 1 is the boundary separating the epidermis from the dermis layer of the human skin. The keratinocyte stem cells which are mostly found at the basal lamina begin cell proliferation in the basal layer and undergo keratinocyte differentiation until reaching the granular layer. The basal layer appears to be columnar in shape and consists of keratin filaments around its nucleus, hemidesmosomes and desmosomes. Hemidesmosomes and desmosomes are both cell attachment sites but differ in what they bind to. The hemidesmosomes attach one cell to the extracellular matrix whereas the desmosomes attach two cells together. Keratin filaments are elastic fibrous proteins and are normally

expressed during keratinocyte differentiation. The keratinocytes at the basal layer express keratin 5 and keratin 14. From the basal layer to the spinous layer during differentiation, the expression of keratin switches to keratin 1 and keratin 10.

The spinous layer which is situated above the basal layer has a spinelike appearance at its borders because of the several desmosomes. Lamellar bodies are synthesized in the spinous layer of the epidermis and is important for the secretion of intercellular lipids which contributes to the barrier function of the cornified layers (5). The lamellar bodies consist of various components such as lipids, protease inhibitors, antimicrobial peptides and corneodesmosomal proteins. From electron microscopy images, the lamellar bodies appear to be round granules of 300-400 nm in length and 100-150 nm in width. A decrease in calcium or potassium across the epidermis initiates the secretion of the lamellar bodies (6). Lamellar bodies are also found in the granular layer of the epidermis.

The granular layer of the epidermis has three layers and is denoted as SG3, SG2 and SG1 (7). In the SG3 layer which is the layer closest to the spinous layer, keratohyaline granule (KHG) is gradually synthesized in the cytoplasm. It is a granule that is composed of keratin and keratin-binding proteins such as profilaggrin. The keratinocyte in the SG1 layer of the granular layer closest to the cornified layer undergoes cell death and form the dead cell layer which migrates to the cornified layer. The cell death of the keratinocyte cell in the SG1 layer is referred to cornification instead of apoptosis. An increase in intracellular calcium ions induces the termination of keratinocyte differentiation during the SG1 to cornified layer transition and a study done by Hennings et al. 1980 (8) classified 1.2 mmol/litre of calcium ion as being the signal for terminal differentiation.

Cornification begins to occur in the transition layer as illustrated in figure 1 because the keratinocyte cell makes a transition to corneocyte due to the keratinocyte cell losing all its content, and the aggregation of keratin gives the corneocyte its shape. The corneocytes are held together by proteins known as the corneodesmosomes. The cornified layer is usually described in appearance as the "bricks and mortar" model where the bricks are the corneocytes and the intercellular lipid is the mortar (9). Moreover, a study conducted by Steinert et al. 1981 (10) demonstrated that the keratin intermediate filament is aligned in parallel arrays. There are three major key events occurring at the cornification process. They are the formation of intracellular keratin network, formation of the cornified envelope and the formation of intercellular lipids. The cornified layer is mainly composed of keratin intermediate filaments, lipids, proteins and natural moisturizing factors (NMF).

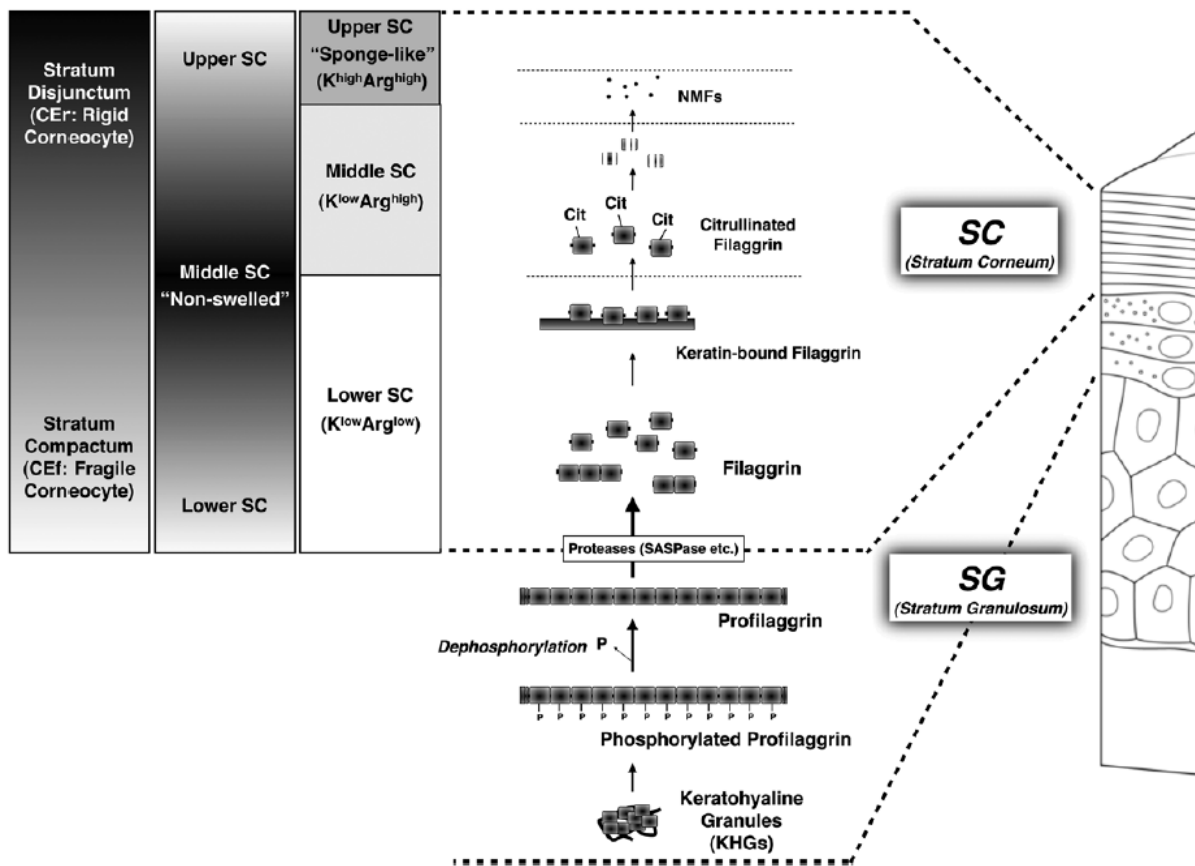


Figure 2 illustrates the pathway of the filaggrin from the stratum granulosum to the stratum corneum of the skin. Within the stratum granulosum layer, profilaggrin is released from the keratohyaline granules which is afterwards dephosphorylated and cleaved forming filaggrin in the stratum compactum zone of the stratum corneum. The newly synthesized filaggrin form the keratin-filaggrin complex together with the keratin filaments. The keratin-filaggrin complex is then citrullinated in the middle stratum corneum which causes the filaggrin to be release from the complex. The released filaggrin is then attacked by protease caspase-14 forming small peptides. The small peptides are then further degraded in the stratum disjunctum zone of the stratum corneum forming the natural moisturizing factors (NMF) (Matsui et al. 2015)

The cornified layer consists of 10-20 piled up layers of SG1 dead cells and a single corneocyte can be 10-30 μm in diameter and 1 μm thick (11). The cornified layer does not consist of homogenous corneocyte cells within its layer and there is evidence that indicates that the cornified layer has three distinct zones. Scanning electron microscopic technology was performed against several human skin samples to observe the three hydration zones based of their swelling potential in 5-20% salt solutions (12). The lower cornified layer which is closest to the granular layer denoted as the stratum compactum, has fragile corneocyte cells, are small and less hydrophobic compared to the zones above. The upper cornified layer denoted as stratum disjunctum has on the other hand large, hydrophobic and rigid corneocyte cells. Time-of-flight secondary ion mass spectrometry was used to confirm the hypothesis of the three hydration zones of the stratum corneum by comparing the ions concentration within the stratum corneum (13). An illustration of the three zones of the stratum corneum layer together with the processing of filaggrin within each zone is shown in figure 2.

The aggregation of the keratin filament is caused by a protein known as the filaggrin which is originated from the profilaggrin situated in the granular layer. Profilaggrin and filaggrin are important proteins for the stratum corneum formation (14). When profilaggrin is released from the keratohyaline granules from the granular layer, it is dephosphorylated and cleaved by proteases forming filaggrin in the lower zone of the stratum corneum. The newly synthesized filaggrin then assembles with the keratin fibers forming macrofibrils giving the corneocyte its shape. A study conducted by Steinert et al. 1981 (10) demonstrated that an optimal ratio of two moles of filaggrin to three moles of keratin filament make up the macrofibrils. In the middle zone of the stratum corneum, the filaggrin-keratin complex is citrullinated by peptidylimides which leads to the release of the filaggrin from the complex. The released filaggrin is then attacked by the protease caspase-14 forming small peptides. The peptides are then further degraded by breomycin hydrolase forming several amino acids such as natural moisturizing factors (NMF). The natural moisturizing factors (NMF) contribute to water retention because the amino acids are insoluble, and also protects against UV light.

Desmosomes

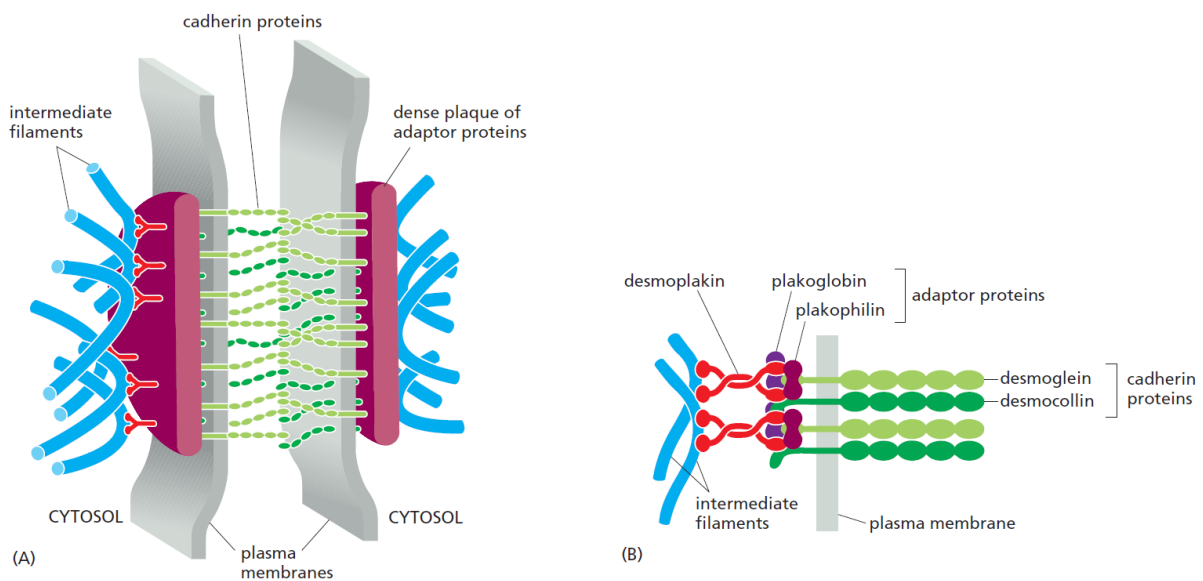


Figure 3 illustrates the components of the desmosomes. The image (A) represents the structural components of the desmosome. The image (B) represents the molecular components of the desmosome such as the intermediate filaments, the adaptor proteins and the cadherin proteins. ISBN 978-0-8153-4464-3 Page 1046

Desmosomes are intercellular adhesive proteins that are characterized as cellular spot welds by histologists (15). Desmosomes consist of three major gene families which are the cadherins, armadillo proteins and plakins. The desmogleins (Dsgs) and the desmocollins (Dscs) are transmembrane members of the cadherins and their cytoplasmic tails provide binding sites for the armadillo proteins which are the plakoglobin (PG) and the plakophilins (PKPs). The plakins family like the desmoplakin (DP) on the other hand links the cytoplasmic intermediate filaments (IF) to the cadherin-armadillo complex (figure 3).

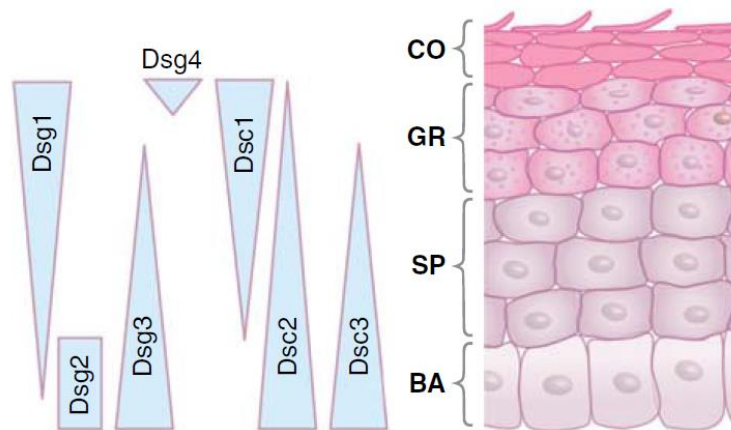


Figure 4 illustrates the specific isoform of desmosomal cadherins along the layers in the epidermis. The epidermis consists of different layers such as the basal (BA), spinous (SP), granular (GR) and cornified (CO) layers. The amount of desmoglein 1-4 (Dsg1-4) and desmocollin 1-3 (Dsc1-3) expression is shown like the pale blue diagrams. (Green et al. 2007)

Structural variations of the desmosomes have been observed by electron microscopy and thus leading to the idea that desmosomes in distinct layers of the epidermis vary in size and appearance. During epidermal differentiation, desmosomes at the basal layer increases in size and become more electron-dense as they travel to the cornified layer. The article from Green et al. (15) states that the cadherin proteins such as the desmoglein and the desmocollin are the adhesive “core”. Specific amount of the different isoform of desmoglein and desmocollin are located in different layers of the epidermis (figure 4). As the desmoglein 1 (Dsg1) at the basal layer ascend to the cornified layer, its amount expression increases. Desmoglein 2 (Dsg2) is only found in the basal layer. The expression of desmoglein 3 (Dsg3) is large at the basal layer but decreases during the epidermal differentiation. Desmoglein 4 (Dsg4) is concentrated in the granular and cornified layer.

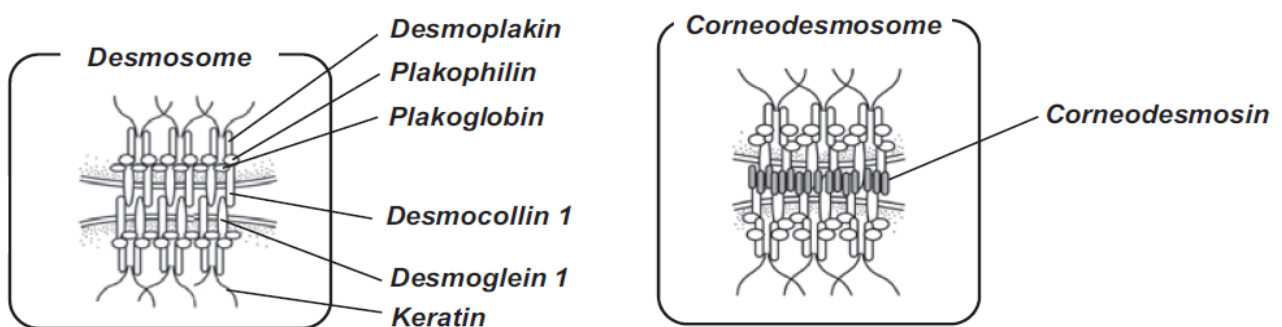


Figure 5 illustrates the difference between desmosome at the granular layer and corneodesmosome at the cornified layer. Both images show the intermediate keratin filaments, the adaptor proteins and the cadherin proteins. The only difference between the desmosome and the corneodesmosome is the binding of the corneodesmosin to the cadherin proteins in the intercellular space. (Matsui et al. 2015)

During the last phase of the keratinocyte differentiation at the cornified layer of the epidermis, the desmosomes from the granular layer are modified into corneodesmosomes. The corneodesmosomes contain corneodesmosin which is a unique extracellular component in the adhesive structure of the cornified layer in the epidermis. The corneodesmosome consists of desmoglein 1, desmocollin 1 and corneodesmosin

illustrated as in figure 5. For the process of desquamation to occur, the desmoglein 1, desmocollin 1 and corneodesmosin from the cornified layer are cleaved by the enzymes kallikreins and cathepsins. The corneodesmosin and the desquamation enzymes are stored in lamellar granules which are typically found in the spinous and granular layer. The lamellar granules fuse to the plasma member of the keratinocyte cell of the granular layer and secrete their content into the intercellular space which results in the formation of the corneodesmosome.

Cholesteatoma

Cholesteatoma is keratinizing squamous epithelium growth disorder which destroys bony structures in the middle ear. Cholesteatoma leads to complications such as hearing loss, vestibular dysfunction, facial paralysis and intracranial complications. The cholesteatoma can be classified in two classes; the congenital and acquired which are divided in classes because of their different origin. Although two classes of the disease exists, they share the same molecular mechanism (16). Even though there are many published data on the cholesteatoma so far, there are still many questions about the molecular mechanisms of cholesteatoma that remain unclear. Cholesteatoma does not metastasize and its formation appears to be related to dysfunctional internal molecular mechanisms or external factors such as pro-inflammatory cytokines, growth factors or bacterial toxins (17).

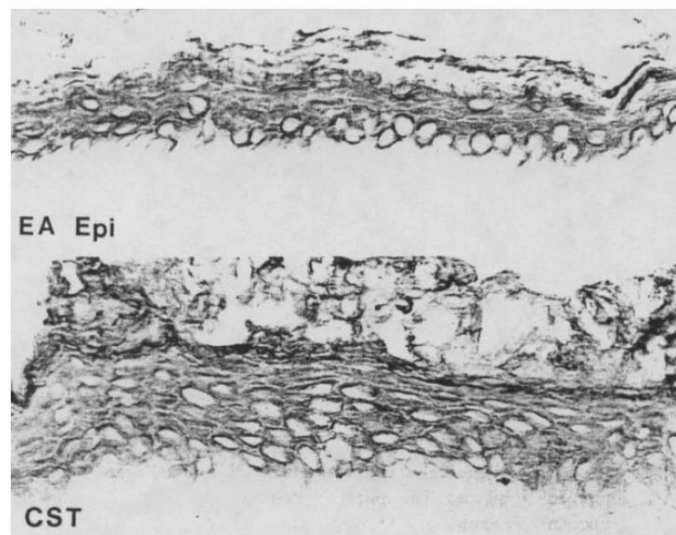


Figure 6 illustrates the comparison of keratin 10 expression for the skin of the external auditory meatus (EA Epi) and cholesteatoma (CST) done by Lee et al. 1991. Both the skin and cholesteatoma were stained by monoclonal antibody against keratin 10. Keratin 10 is generally paired with keratin 1 and thus the use of either keratin 10 or 1 will give the same results.

Based on a study done by Lee et al. 1991 (18), the cholesteatoma closely resembles the skin of the external auditory meatus. Cytokeratin expression pattern varies within the epithelium and thus Lee et al. 1991 used

monoclonal antibodies staining techniques to determine the position of the several class of cytokeratin within the epithelium. The skin of the external auditory meatus and cholesteatoma were stained by monoclonal antibody against keratin 10. The cytokeratin consists of at least 19 different polypeptides and keratin 10 is generally paired with keratin 1 which will yield the same results if either keratin 1 or 10 were to be used. Figure 6 shows that the structures in both the skin and the cholesteatoma are almost identical.

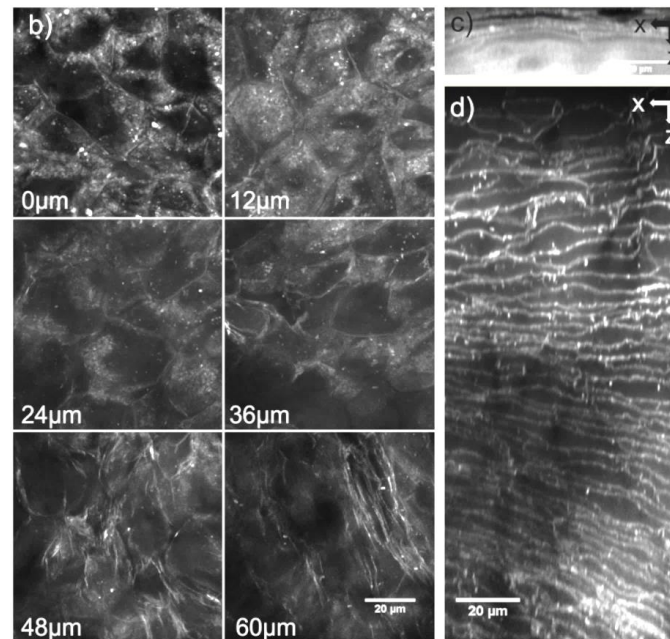


Figure 7 illustrates the structures in a non-sliced cholesteatoma sample during CARS microscopy. The entire piece of cholesteatoma sample was only frozen after surgery and afterwards used for imaging. Images b) are images in the x-y plane in different depth of the cholesteatoma matrix. Images c) and d) are images in x-z plane of the cholesteatoma skin. Image acquired by Jonathan Brewer (brewer@memphys.sdu.dk).

The image of figure 7 was acquired by my supervisor Jonathan Brewer and illustrates the lipids structures in a piece of cholesteatoma which was not sliced. Another study done by Bloksgaard et al. 2012 (2) showed that the lipid composition from the cholesteatoma resembles the stratum corneum of the skin. Techniques such as multiphoton excitation fluorescence microscopy and high-performance thin-layer chromatography were used to compare the cholesteatoma and the skin. The results from the article showed that the cholesteatoma has a thicker stratum corneum-like region than the stratum corneum from the skin. They also demonstrated that cholesteatoma is exactly organized like the skin stratum corneum. This lead to the deduction that the cholesteatoma may also possess a defensive/permeability barrier as the skin.

Material and method

The present study was approved by the Ethical Comity of Region Syddanmark, (reference ID S- 20120062). Written informed consent was obtained for all cholesteatoma patients. Patient consent for the skin tissue samples was not required, because Danish regulations consider human tissue left over from surgery as discarded material. All clinical investigations were conducted according to the principles expressed in the Declaration of Helsinki. The procedures mentioned below were applied to both the human skin and the cholesteatoma skin sample.

Freezing of sample

Material: Liquid nitrogen, dry ice, 2-methylbutane, tissue-tex

A container filled with liquid nitrogen together with a beaker of 2-methylbutane was prepared to submerge the sample. The sample was first dipped into tissue-tex so as to protect the sample from dehydration and to prevent the lipids in the sample dissolving in the 2-methylbutane. The sample was then placed in the beaker containing 2-methylbutane for about 1 minute maximum. The frozen sample was afterwards placed in a container, labeled and kept at -80°C in the storage room.

Slicing of tissue samples

Material: Cover slide 50×24 mm, PBSx10 (5mL), BSA (500 mg), SA (25 mg), milliQ water (45 mL), poly-lysine solution, Methanol (MeOH)

The frozen sample prepared from the above procedure is sliced at $20 \mu\text{m}$ thick in the Cryotome machine as illustrated in figure 11. Cover slides were used instead of the normal microscopy slide for STED microscopy because the cover slides are thinner than the microscopy slide and thus would give a better image. The cover slide was first coated with poly-lysine solution for about 5 minutes, rinsed in PBS/BSA/SA solution and air dry for 2 hours. Phosphate buffered saline abbreviated as PBS is a buffer solution used for hydrating and washing the sample because its osmolarity and ion concentrations resembles the human body and thus is non-toxic to most cells. Bovine serum albumin abbreviated as BSA acts as a blocking buffer which blocks the reactive sites to which primary

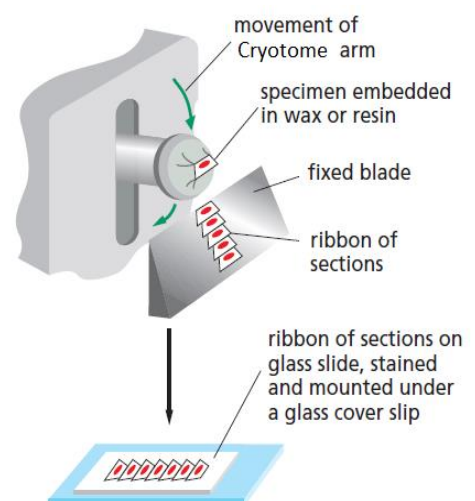


Figure 8 illustrates the slicing of tissue sample by the Cryotome machine. The sample from the freezing process is embedded in tissue-tex at the Cryotome arm. The sample is then sliced by the fixed blade and mounted on a microscopy slide by contact. ISBN 978-0-8153-4464-3 Page 535

and secondary antibodies may bind unspecifically. This helps in eliminating background staining. The polylysine solution allows better contact between the cover slide and the sample. After slicing through the fixed blade, the 20 µm thick sample was transferred to the cover slide by contact. The presence of the sliced sample was then checked under a light microscope. Afterwards, the sample was submerged in MeOH for 10 minutes in -20°C. For confocal and CARS microscopy, normal microscopy slide were used.

Labeling with TopFluor dye

Material: 0.8% Topfluor dye, PBS/BSA/SA solution, PBS solution, Prolong Gold, Aluminum foil

The 20 µm thick sample was rinsed in PBS buffer solution. A magic marker was used to draw a circle around the sample so as to keep the labeling solution enclosed on the sample. A diluted solution of 0.8% of TopFluor dye was prepared with the PBS/BSA/SA solution. 50 µL of the diluted TopFluor dye was added on the sample and kept overnight at room temperature. The sample was wrapped in aluminum foil to protect the sample from light. After an overnight exposure in the dye, the sample was rinsed in PBS solution and was submerged in the solution for 15 minutes. After the 15 minutes, the PBS solution was removed and the cover glass was mounted using Prolong Gold medium.

Indirect immunocytochemistry

Material: 1% SDS in PBS, 1% primary antibody (Cytokeratin I, desmoglein I and filaggrin), 1% secondary antibody (Abberior Star 440sx, Abberior Star 488), PBS/BSA/SA solution, Prolong Gold, cover glass 18 mm diameter

Antibodies are the main components used to detect specific target molecules such as antigen in a process known as indirect immunocytochemistry. The antibodies are unique proteins that are produced by the immune system in billions of different forms with specific binding sites to specific antigen. The unique characteristic of the antibodies is therefore a powerful tool to detect the desired specific proteins such as the cytokeratin 1, desmoglein 1 and filaggrin for this experiment. In the indirect immunocytochemistry process, two antibodies are used to investigate the desired protein in the cell. A stronger fluorescent signal is achieved when an unlabeled primary antibody is linked and detected by labeled secondary antibodies. The primary antibody first binds to the specific desired antigen in the cell and afterwards the secondary antibodies binds to the primary antibody. The secondary antibodies which are covalently coupled to a marker molecule such as fluorescence labels make the antigen-antibody complex readily detectable by the microscope. The detection in this process is sensitive as several secondary antibodies binds to a single primary antibody leading to a strong fluorescence signal.

The sample was washed 5 times for 3 minutes in PBS/BSA/SA solution and afterwards the primary antibody was applied for 1 hour. After the 1 hour, the sample was washed for another 5 times for 3 minutes with the PBS/BSA/SA solution and then the secondary antibody was applied for another 1 hour. The sample was washed again 5 times for 3 minutes with the PBS/BSA/SA solution. The sample was then air dry and a drop of Prolong Gold was applied on the sample so as to prevent oxygen from interfering with the sample. Oxygen can cause photo bleaching and Prolong Gold minimizes this effect. On the cover slide/microscopy slide we therefore had a sandwich of the sliced sample, Prolong Gold medium and cover glass. The sample was then stored at room temperature in aluminum foil to keep away from light. Control measurements on the samples involving only the labeling of the secondary antibodies was performed in previous studies and negative labeling in the samples indicated that the secondary antibodies did not bind to unspecific binding site in the samples. (Data not shown)

Confocal fluorescence microscopy

The confocal microscopy is an imaging technique which is advantageous to use compared to conventional widefield microscopy because the confocal microscopy can control the depth of the field and eliminate background information from the focal plane. Analysis of optical sections can be used to analyze thick specimen ranging up to 100 μm . The confocal microscopy provides optical resolution in both the axial (z) and lateral (x and y) plane which makes a 3D image possible. The basis for confocal microscopy is using the pinhole aperture which is placed in front of the detector to remove the out of focus light. Laser light is emitted by the laser excitation source and passes through a pinhole aperture. Only emitted fluorescence light from the in-focus point is focused through the pinhole and contributes to the final image. The emitted light from out of focus regions in the specimen is not focused down through the pinhole and is rejected by the pinhole and thus is excluded from the final image. Details about the principle behind the confocal microscopy can be found in the article Claxton et al. 2006 (19).

STED microscopy

STED microscopy stands for **ST**imulated **E**mission **D**epletion microscopy and is a superresolution technique used to obtain images which can be resolved below the 200 nm limit. In normal defraction limited microscopy, two point sources that are about 200 nm apart can still be resolved but if they are less than 200 nm apart, they will overlap and will not be resolved. STED microscopy generates an image by reducing the size of the point spread function. The size of the region can be as small as 20 nm in biological specimen.

Two lasers known as the excitation and depletion laser are used in STED microscopy. The principle behind STED microscopy is that the excitation laser excites fluorophores in a given area and the depletion laser which has an intensity profile shaped like a torus (dough-nut shape), de-excites some of the fluorophores through simulated depletion. The depletion laser effectively confines the emitted fluorescence to the central part of the torus and thus gives a smaller fluorescence spot which can be as small as 20 nm (ISBN 978-0-8153-4464-3). This technique can thus be used to resolve images of fluorescence molecules that are less than 200 nm apart. Details about the principle behind the STED microscopy can be found in the article Farahani et al. 2010 (20).

CARS microscopy

CARS microscopy stands for coherent anti-Stokes Raman microscopy and is a label-free imaging technique which allows the study of cell structures. CARS images are obtained based on the specific vibrational signatures of molecules because chemical bonds within the molecules have unique motions occurring at specific vibrational frequencies. CARS is a more advantageous technique to visualize structures in biological samples compared to conventional techniques because it allows direct visualization of the molecules of interest. This is in contrast to fluorescence microscopy where one must label the sample with a fluorophore. Also time can be spared from labeling the samples and fluorescence dyes bleach over time. The labeling process of biological samples can cause phototoxicity and harm the biological specimen which may affect the results of the experiment.

The principle behind the CARS microscopy is that two lasers known as the pump (ω_p) and Stokes (ω_s) beam are combined and directed to the microscope and directly focusing into the samples as shown in figure 9. By tuning the energy difference between the pump and the Stokes beam, it is possible to tune into specific vibrational energies characteristic for specific molecules. Emitted photons are collected by the condenser forward-detected CARS (F-CARS) from the detector PMT1 or by the focusing objective for epi-detected CARS (E-CARS) from the detector PMT2 (21). Detailed theory of the CARS microscopy can be found in the Potma et al. 2004 article (22).

A z-stack of the sample was taken by each type of microscopy mentioned above and an ideal image was selected for analysis. The brightness and contrast were adjusted to an ideal image by the program ImageJ and the "plot profile" option from the program ImageJ was used to measure the gray value for comparison.

Results

Control

The following results for the control in the cholesteatoma and the human skin are presented by using the CARS set up on unlabeled samples. The images from figure 9 was obtained by two photon excitation fluorescence microscopy using CARS set up and illustrates autofluorescence exhibiting from both the cholesteatoma and the human skin. The diagrams from figure 9 are control measurements done by the program ImageJ to differentiate between autofluorescence and labeling.

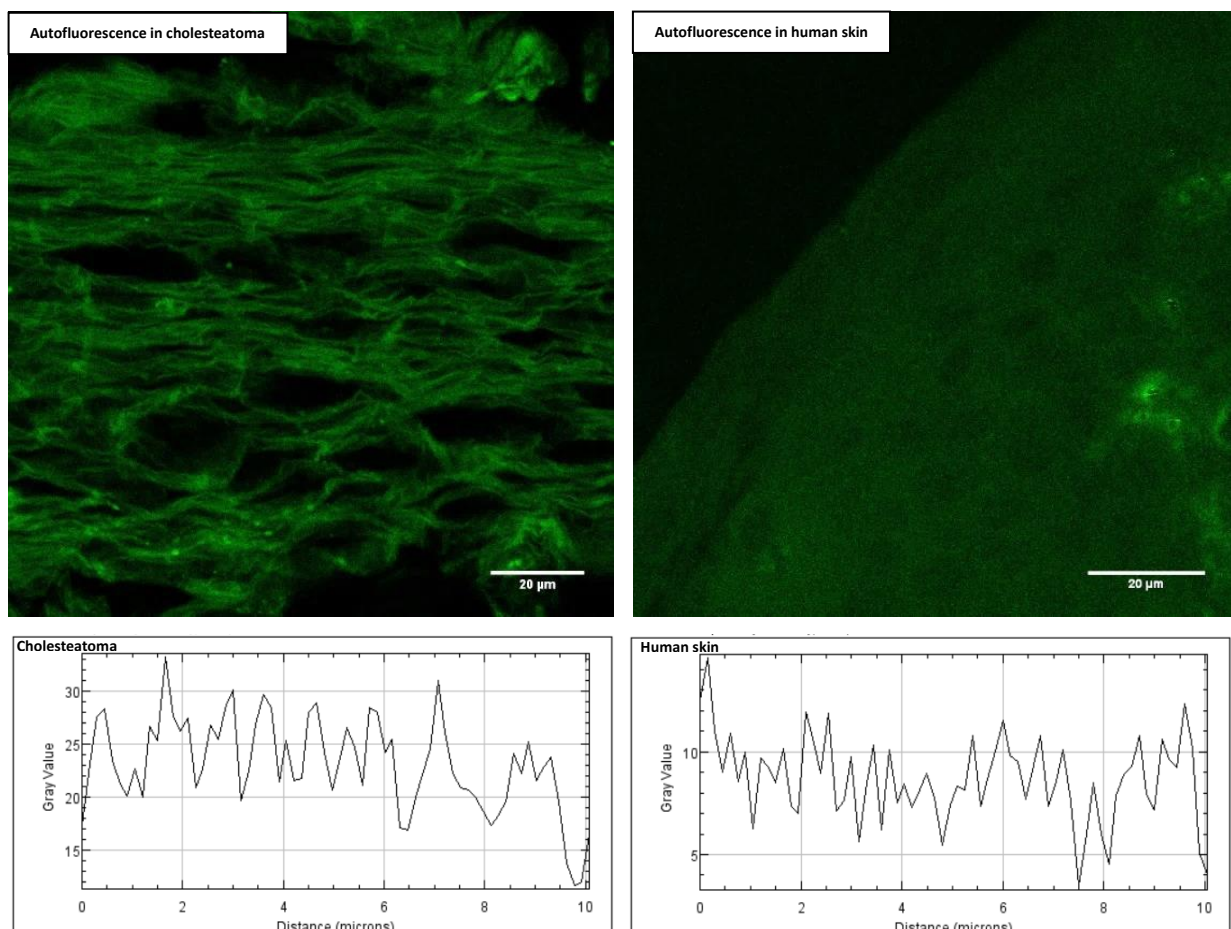


Figure 9 illustrates an image of the control for the presence of autofluorescence in cholesteatoma and human skin, by the two photon excitation fluorescence microscopy using the CARS set up. The cholesteatoma and human skin samples were not labeled by any fluorophores or antibodies and are 20 μm thick. The diagrams below the images are gray value plots obtained from the program ImageJ to measure the grey values at a certain position in the image. The scale bars are both at 20 μm.

Care was taken to match the acquisition settings of the control samples with the labeled samples. This included the laser intensity, pixel size, and acquisition time. In this case a line average of 5 was used together with an accumulation of 1. The line average is when each line of the image is scanned several times and the data for each point is averaged to reduce noise. The line accumulation on the other hand is the summing up of the pixel intensity of each line which was scanned several times. To enhance the visualization of the

images, the brightness and contrast were adjusted to a typical image by the program ImageJ. The “plot profile” option from the program ImageJ was used to measure the gray value for the autofluorescence in the samples. The grey value for autofluorescence in cholesteatoma is about three times than that found in the human skin and their values are around 25 and 8 respectively (figure 9). The presence of autofluorescence in both the cholesteatoma and the skin is detected. The autofluorescence image of the cholesteatoma appears as not organized parallel array of fibers across the whole cholesteatoma sample. The autofluorescence image in the skin on the other hand seems to have undefined structures across the whole skin sample.

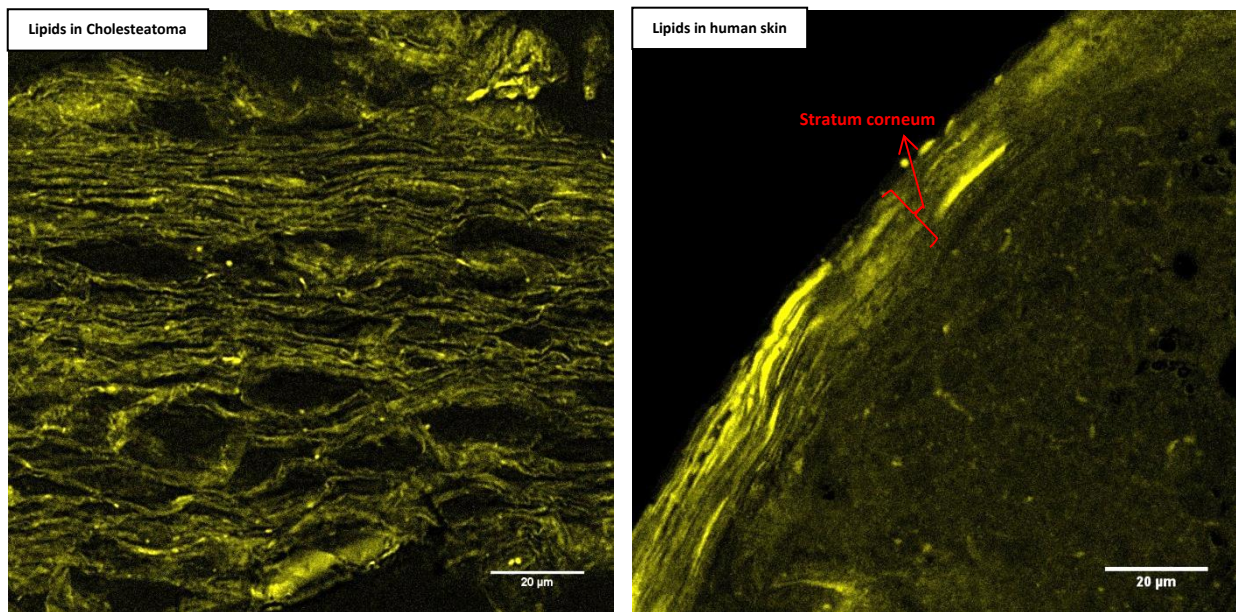


Figure 10 illustrates an image of the control for lipids in cholesteatoma and human skin by the CARS microscopy. The cholesteatoma and human skin samples were not labeled by any fluorophores or antibodies. The red arrow indicates the stratum corneum section of the epidermis in the skin image. Both scale bars are at 20 µm.

The figure 10 was obtained by the CARS microscopy and illustrates the intercellular lipids in both the cholesteatoma and human skin samples. The lipids image of the cholesteatoma for the control in figure 10 appears to be thick long lines enclosing a dark space between them and is present across the whole cholesteatoma sample. The autofluorescence of the cholesteatoma from figure 9 and the lipids from figure 10 are seen to be co-localized. The control image of lipids for the skin on the other hand also appears to have the line structures but is only detectable in the stratum corneum layer of the epidermis. Below the stratum corneum layer, the structures appears to be undefined (figure 10).

Emitted photon is energy difference between two states. Every emission spectrum resulting from different radiated wavelengths, is unique to each element because each different electron transition has specific energy difference. Using this characteristic, an emission spectrum was measured from the control samples of the cholesteatoma and the human skin sample for comparison of their composition. The intensity of the autofluorescence in the cholesteatoma and the human skin were first measured by the “plot profile” option from the program ImageJ. The data obtained was then normalized and plotted in the program SigmaPlot yielding figure 11.

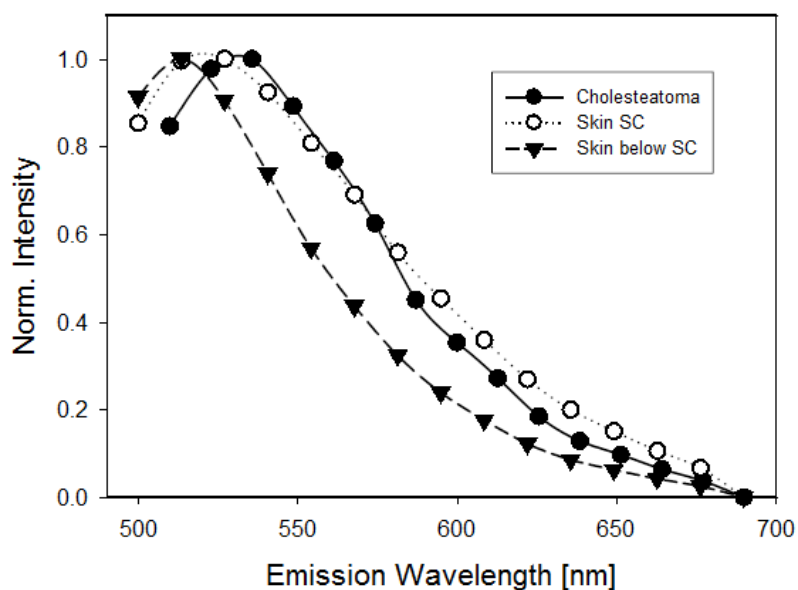


Figure 11 illustrates the emission spectrum of the autofluorescence in both the cholesteatoma and the stratum corneum/below stratum corneum zone of the human skin. The y axis represent the normalized intensity and the x axis represents the emission wavelength.

The figure 11 represents the correlation between the cholesteatoma and the skin stratum corneum, and the cholesteatoma and the layers below the skin stratum corneum. The graph illustrates that the skin epidermis (SC/non-SC) emits the same wavelength until a maximum and decreases at different wavelength. This difference in wavelength indicates that the SC and non-SC composition differs. The cholesteatoma emission wavelength on the other hand starts at a wavelength above the skin’s wavelength until a maximum is reached and follow the same trend as the emission wavelength of the skin stratum corneum. This observation suggests that the composition of the cholesteatoma is almost the same as the composition of the skin stratum corneum.

Labeled lipids images

The figure 12 as follows shows images of cholesteatoma and skin samples which were generated by the STED microscopy for any visualization of structures in the samples. The samples were both sliced at 20 μm thick in the Cryotome and the intercellular lipids were dyed by the fluorescence dye TopFluor.

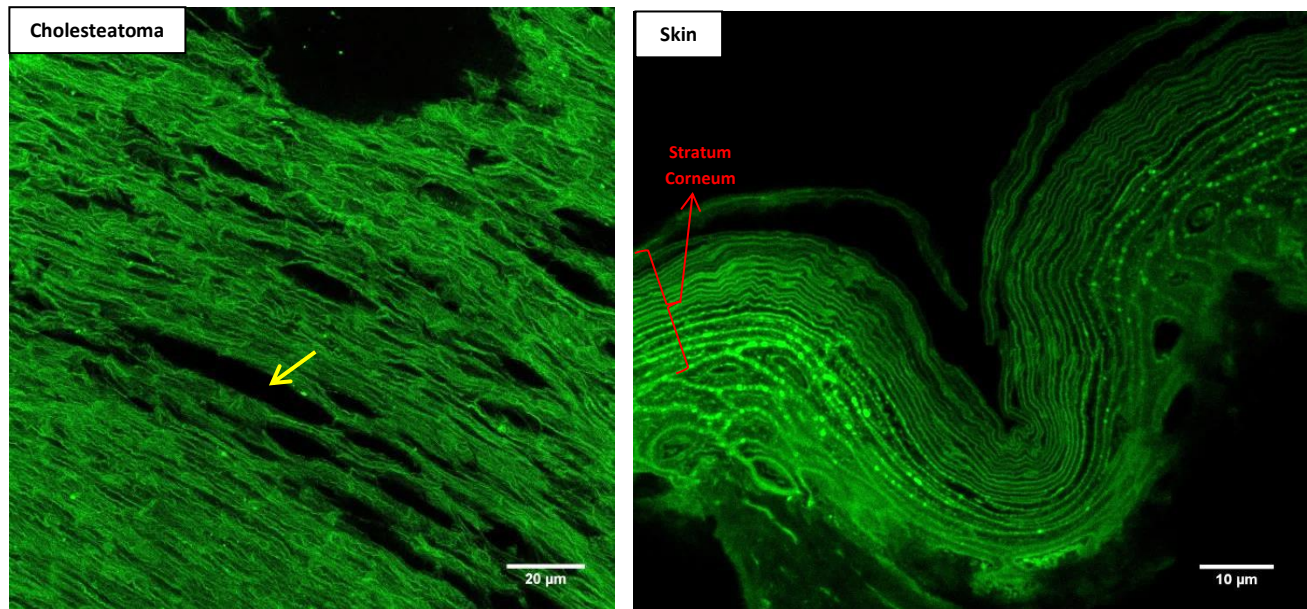


Figure 12 illustrates an image of labeled lipids in cholesteatoma and human skin using the STED microscopy. TopFluor is the fluorescence dye used to dye the lipids in both the cholesteatoma and human skin. The yellow arrow in the cholesteatoma image indicates the corneocyte selected for width measurement. The cholesteatoma scale bar is at 20 μm and the skin scale bar is at 10 μm .

Parallel arrays pattern are detected in both the cholesteatoma and skin images of figure 12. The parallel arrays are the intercellular lipids which enclose corneocyte represented as dark space on the images. In the cholesteatoma image, the corneocytes appear to be more spacious than the corneocytes of the skin which are more tightly pack together. The intensity of the dye appears to fade when reaching upwards to the skin stratum corneum (figure 12). Corneocytes in the outermost layer of the skin stratum corneum appears to have undergo desquamation.

The width of a single corneocyte in the skin stratum corneum of figure 12 was measured in ImageJ and an average of $n=10$ measurements was made. An average value of $0.69\pm 0.16\mu\text{m}$ was obtained for the width of a single corneocyte of the skin (See attachment). The width of a single corneocyte in the cholesteatoma image from figure 12 was also measured in ImageJ and an average of $n=5$ measurements was made. An average value of $1.53\pm 0.27\mu\text{m}$ was obtained for the width of a single corneocyte of the cholesteatoma (See attachment). The large black space in the cholesteatoma image indicated by the yellow arrow in the figure 12 was also measured and a value of $7.17\mu\text{m}$ was obtained.

Cytokeratin I protein images

The figure 13a and 13b as follows illustrate cytoke­ratin 1 images of the cholesteatoma and skin sample by the confocal microscopy and CARS microscopy respectively. The samples were both sliced at 20 μm thick in the Cryotome and labeled by the primary antibody cytoke­ratin I and second antibody Abberior star 488 through the indirect immunocytochemistry process.

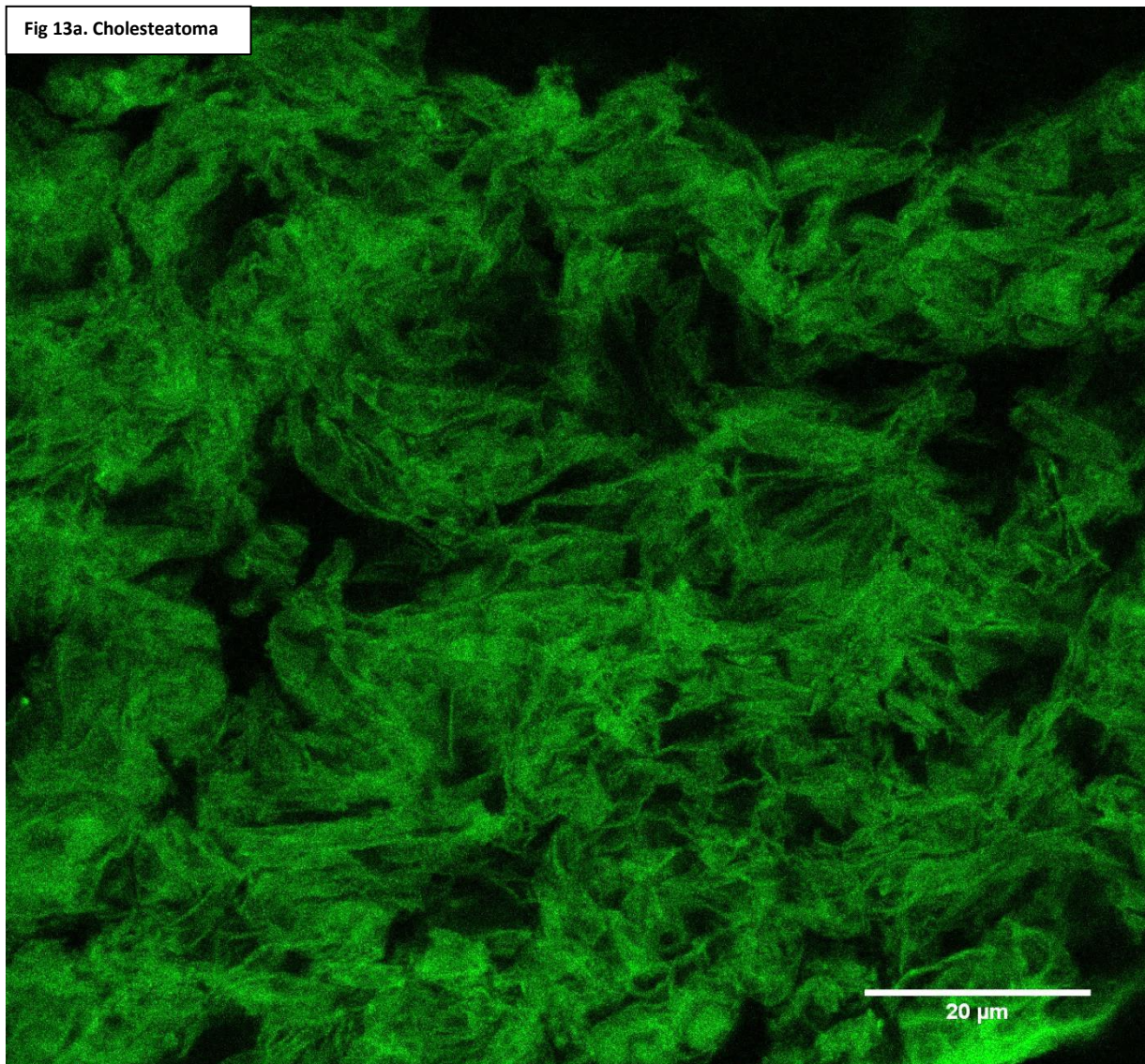


Figure 13a illustrates labeling of cytoke­ratin 1 proteins in the cholesteatoma sample by the confocal microscopy. The cholesteatoma sample was labeled by cytoke­ratin 1 antibodies during the indirect immunocytochemistry process. The scale bar in the images are at 20 μm.

Labeling of cytoke­ratin 1 protein is present in the cholesteatoma image of figure 13a. Parallel arrays of keratin filaments appear to be present but the filaments appear to be very across the whole cholesteatoma sample. The “bricks and mortar” model is hardly seen in figure 13a and the parallel arrays of keratin does not follow the “bricks and mortar” pattern as observed in the control.

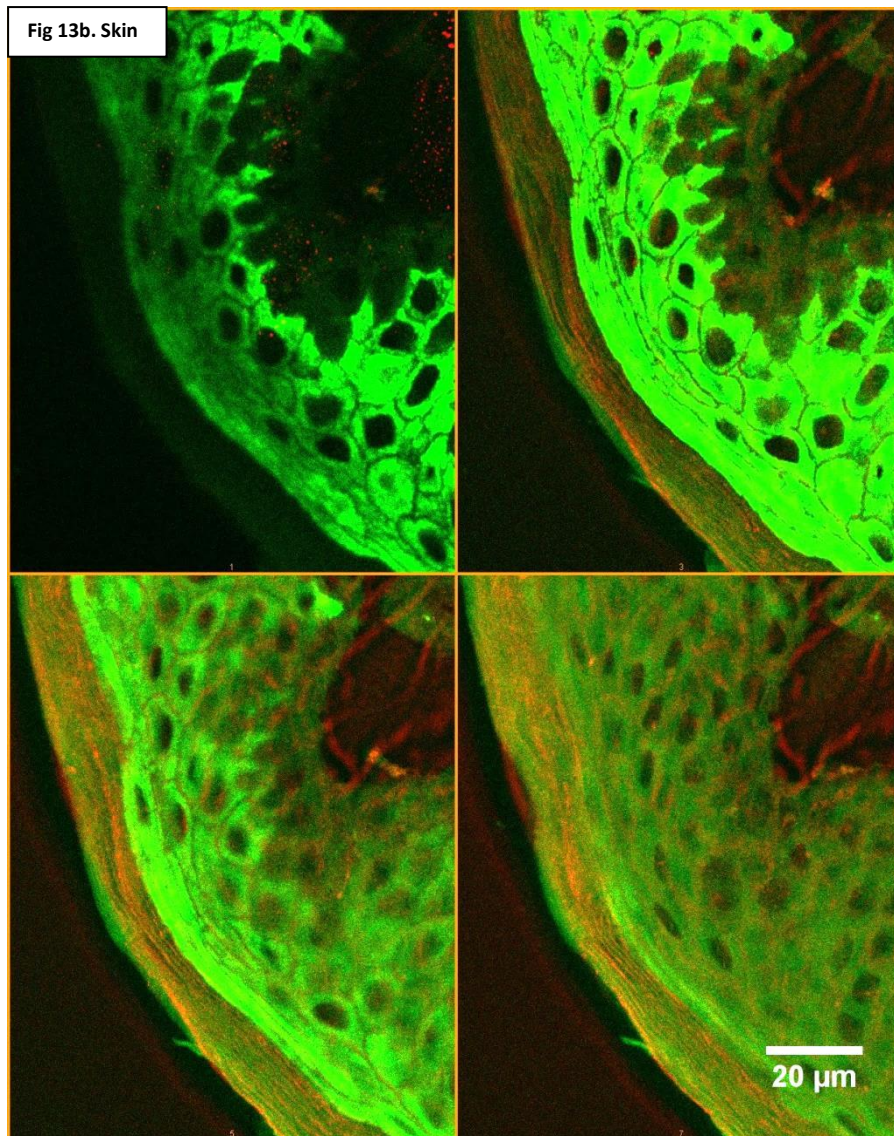


Figure 13b illustrates labeling of cytokeratin 1 proteins in the skin sample by the CARS microscopy. Cytokeratin 1 antibodies were used to label the skin sample. The intercellular lipids and the cytokeratin 1 protein image obtained by the CARS microscopy were made into a composite image by the program ImageJ. The composite image was then made into a montage in ImageJ to visualize the sample through the z-stack starting from left to right of the montage. The red color represents the intercellular lipids whereas the green color represents the cytokeratin 1 proteins. The scale bar is at 20 μm in the image.

Positive labeling of cytokeratin 1 is observed in the skin image of figure 13b and appears to have stronger intensity in the layers below the stratum corneum. Parallel arrays of keratin beside the intercellular lipids can be observed in the stratum corneum although its weak intensity compared to the layers below the stratum corneum. The parallel arrays of keratin form closely pack structures in the stratum corneum.

Filaggrin protein images

The figure 14a and 14b as follows shows images of the cholesteatoma and skin sample generated by the CARS microscopy. The samples were both sliced at 20 μm thick in the Cryotome and labeled by the primary antibody desmoglein 1 and second antibody Abberior star 488 through the indirect immunocytochemistry process.

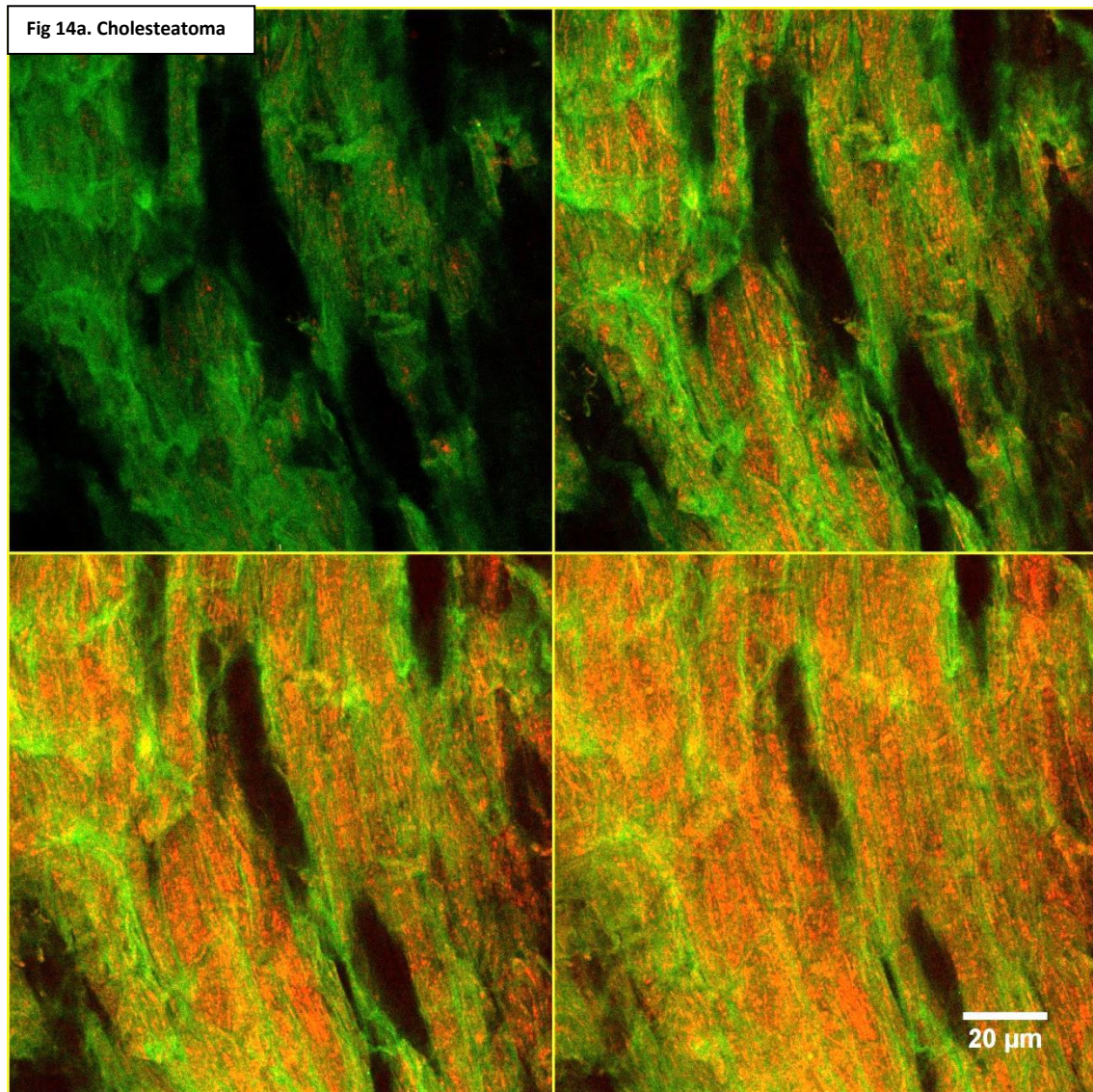


Figure 14a illustrates labeling of filaggrin proteins in the cholesteatoma sample by the CARS microscopy. Filaggrin antibodies were used to label the cholesteatoma sample. The intercellular lipids and the filaggrin protein image obtained by the CARS microscopy were made into a composite image by the program ImageJ. The composite image was then made into a montage in ImageJ to visualize the sample through the z-stack starting from left to right of the montage. The red color represents the intercellular lipids whereas the green color represents the filaggrin proteins. The scale bar is at 20 μm in the image.

Positive labeling of the filaggrin protein is observed in figure 14a. Some parallel array pattern seem to be present beside the intercellular lipids across the whole sample. The “bricks and mortar” pattern is hardly seen in the montage and the black space does not seem to be like typical corneocytes. The black space looks more like gaps than corneocytes.

Fig 14b. Skin

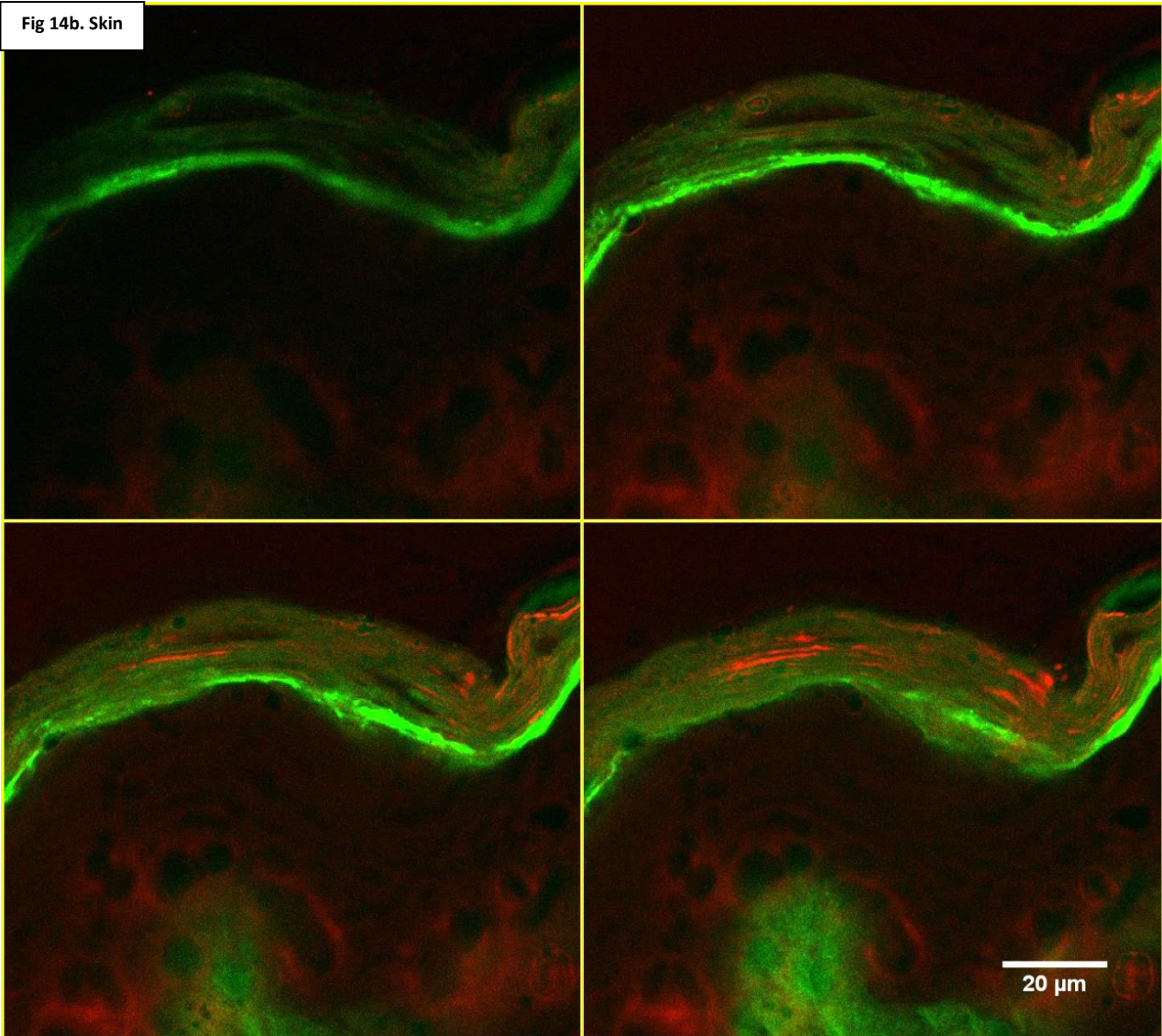


Figure 14b illustrates labeling of filaggrin proteins in the skin sample by the CARS microscopy. Filaggrin antibodies were used to label the skin sample. The intercellular lipids and the filaggrin protein image obtained by the CARS microscopy were made into a composite image by the program ImageJ. The composite image was then made into a montage in ImageJ to visualize the sample through the z-stack starting from left to right of the montage. The red color represents the intercellular lipids whereas the green color represents the filaggrin proteins. The scale bar is at 20 μm in the image.

From left to right of the montage of figure 14b, labeling of filaggrin in the stratum corneum is positive and are situated at the lower zone of the stratum corneum which is as expected. The filaggrin labeling appears as strong intensity of unspecific structure above the granular layer and the intensity appears to diminish when reaching the upper zone of the stratum corneum. Weak filaggrin labeling can also be found in the upper layer of the stratum corneum from the first left image of the montage.

Desmoglein 1 protein images

The figure 15a and 15b as follows shows images of the cholesteatoma and skin sample generated by the STED microscopy and CARS microscopy respectively. The samples were both sliced at 20 μm thick in the Cryotome. A z-stack of the sample was taken by the microscope and a typical image was selected for analysis.

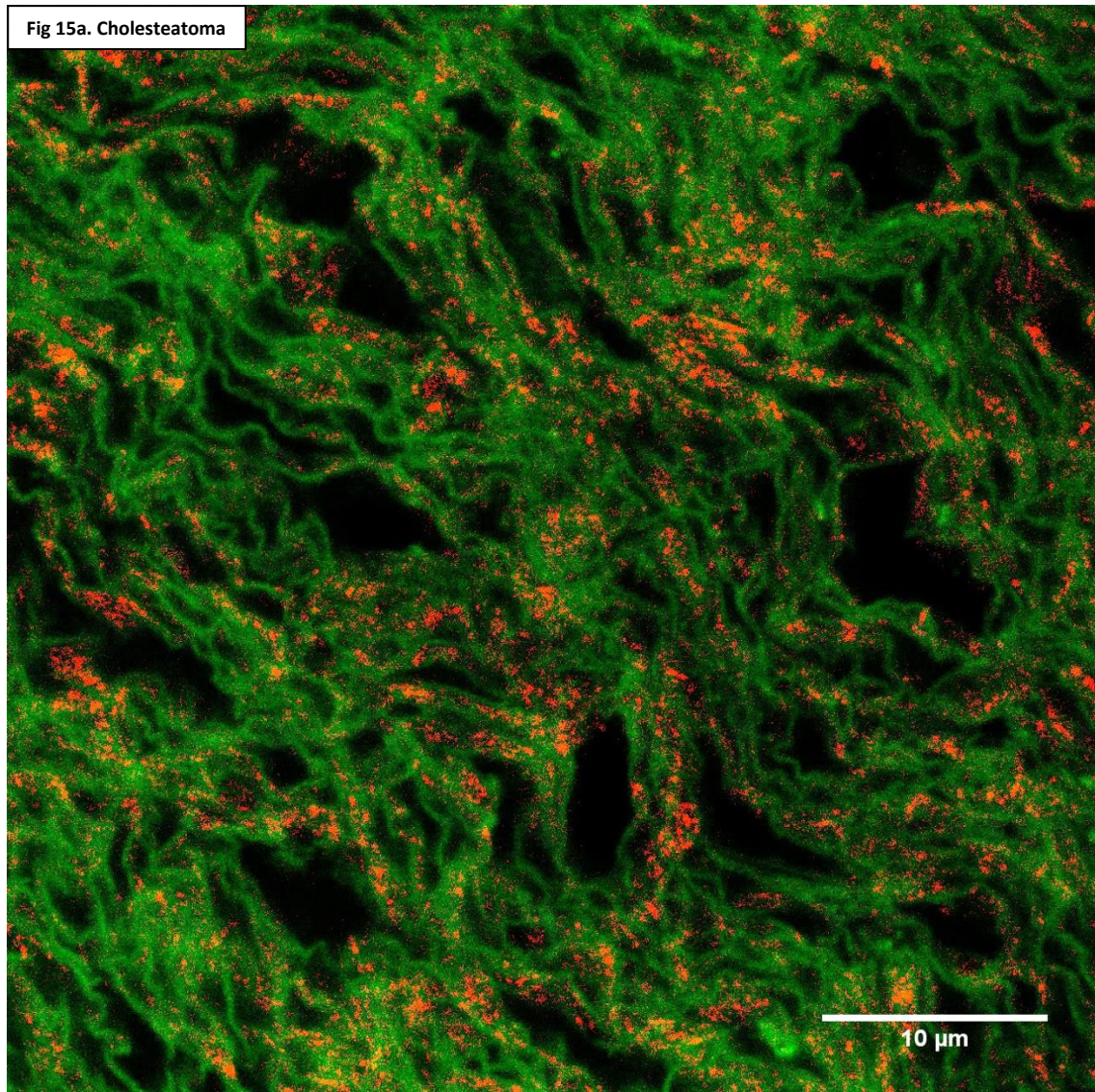


Figure 15a illustrates labeling of the desmoglein 1 protein in the cholesteatoma sample by the STED microscopy. The desmoglein 1 proteins are represented by the red color and the green color is the intercellular lipids. The desmoglein 1 proteins were labeled by desmoglein 1 antibodies and the intercellular lipids were labeled by the TopFluor dye. The scale bar is at 10 μm in the image.

Both the labeling of desmoglein 1 and the labeling of the intercellular lipids are positive in figure 15a. The “bricks and mortar” pattern is observed in the image and the desmoglein 1 is illustrated to function as cellular spot welds holding adjacent corneocyte together. The desmoglein 1 is not typical like the labeling in the skin where one would expect labeling of the desmoglein 1 to be homogenously around corneocytes. Intercellular lipids pattern is observed but appears to be unorganized.

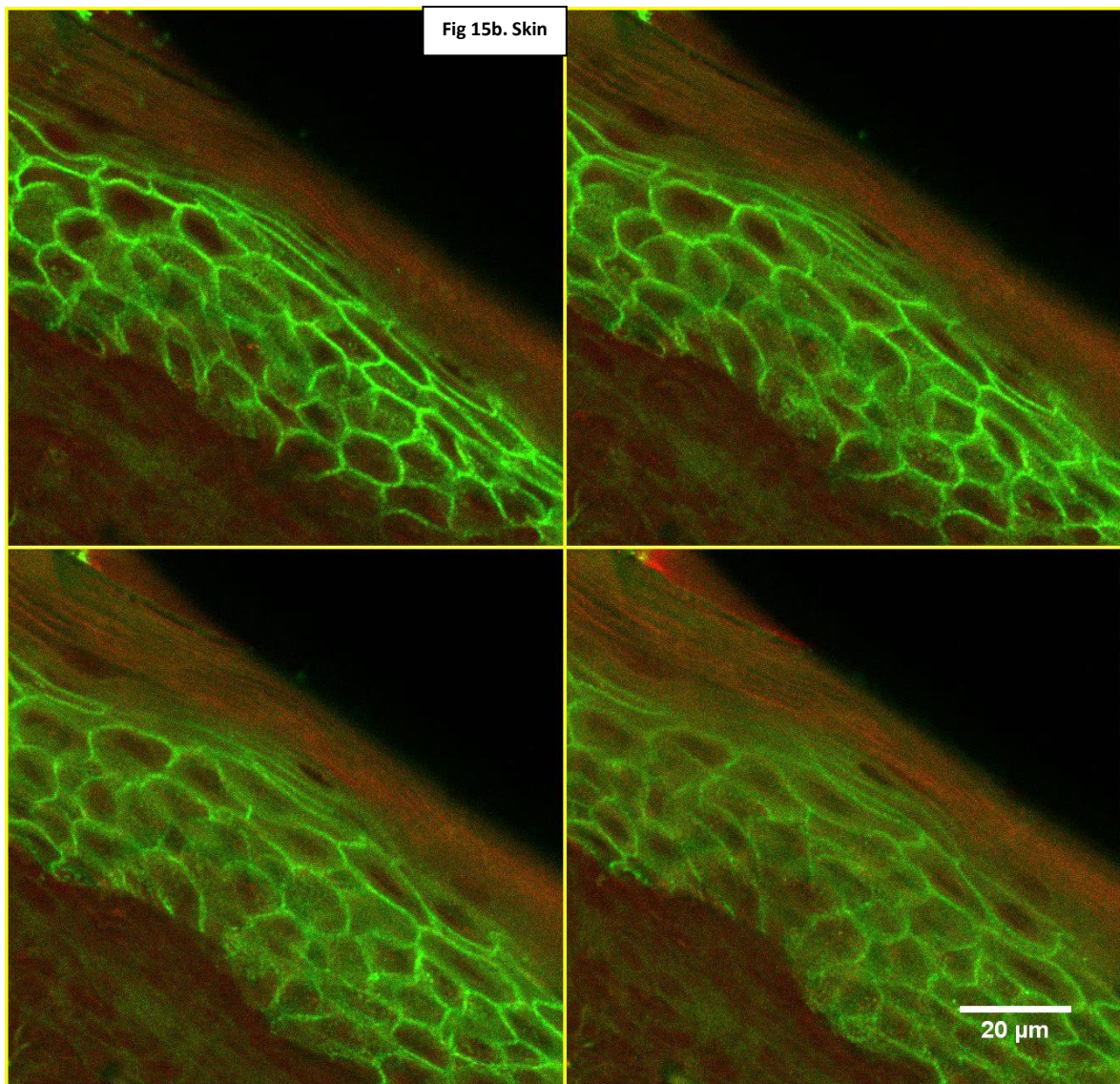


Figure 15b illustrates labeling of the desmoglein 1 protein in the human skin sample using the CARS microscopy. The intercellular lipids and the desmoglein 1 protein image obtained by the CARS microscopy were made into a composite image by the program ImageJ. The composite image was then made into a montage in ImageJ to visualize the sample through the z-stack starting from left to right of the montage. The red color represents the intercellular lipids whereas the green color represents the desmoglein 1 proteins. The scale bar is at 20 μm in the image.

A composite image of desmoglein 1 and lipids is illustrated in the cholesteatoma image of figure 15 because it is difficult to have a good perspective of the structures if only desmoglein 1 were shown. The red color represents the desmoglein 1 and the green color is the lipids. The desmoglein 1 proteins appear to have dot-like shapes and are within the long lipids linings. The desmoglein 1 of the skin image from figure 15 appears as a straight line because CARS microscopy does not resolved the image as STED microscopy does and thus the several desmoglein 1 proteins closed to one another appear as one.

Discussion

Skin

In figure 12, the “bricks and mortar” model as referenced in the theory section can be observed in the STED image of the skin. The intercellular lipid appears as parallel arrays pattern and the dark spaces between the intercellular lipids are considered to be the corneocyte. The skin image in figure 12 thus confirms the basic structure of the “bricks and mortar” model as presented in Menon et al. 2012 (9). The STED microscopy image from figure 12 provided the best image among the other techniques because STED microscopy can resolve images below the 200 nm limit and can resolve region as small as 60 nm (0.06 μm) in skin. This enables us to resolve the structure of the intercellular lipids, something which has been possible to do before using transmission electron microscopy. An average width of a single corneocyte was calculated from a 10 layers corneocyte at figure 12. The widths of the corneocytes were measured, and an average width of $0.69 \pm 0.16 \mu\text{m}$ was obtained (See attachment). The result of 0.69 μm correlates with the data shown in Marks et al., 1983 (11) where it is demonstrated that the thickness of a single corneocyte is less than 1 μm .

Cytokeratin 1

Parallel arrays of keratin filaments besides the intercellular lipids can be observed in the cytokeratin 1 image montage at figure 13b. The results seen in figure 13b coincide with a study conducted by Marks et al., 1983 (11) where he described the keratin filaments in the stratum corneum to be aligned in close proximity in parallel arrays. In figure 13b, the cytokeratin 1 proteins labeling is not observed in the basal layer of the epidermis. The presence of cytokeratin 1 proteins is seen to be situated only in the outer layers of the epidermis which confirms the theory describing that keratin 1 is usually expressed during keratinocyte differentiation from the spinous layer of the epidermis. Labeling in the stratum corneum is poor compared to the labeling in the layers below the stratum corneum.

Filaggrin

In figure 14b, a bright area of the filaggrin labeling can be observed at the lower zone of the stratum corneum which indicates that the filaggrin proteins are synthesized in the lower zone of the stratum corneum. The observation made from figure 14b correlates with the theory described in the theory section and also confirms the study conducted by Manabe et al. 1991 (23) where the localization of filaggrin and its relation to the keratin filaments were investigated. In figure 14b, some weak labeling of the filaggrin can be observed in the upper layers of the stratum corneum which is not as expected in accordance to the study from Manabe et al. 1991. In the article, Manabe et al. claimed that the filaggrin disappears when reaching the upper zone of the stratum corneum and set the keratin filaments loose. A possible explanation to the issue from figure 14b could be that the antibody can still bind to fragments of degraded filaggrin.

Desmoglein 1

In figure 15b, strong desmoglein 1 labeling can be observed in the areas below the stratum corneum where the desmoglein 1 is present in the intercellular space among keratinocyte. This observation correlates with the theory described above where the desmoglein 1 which is a component of the desmosome, is an intercellular adhesive protein. However, the expression of the desmoglein 1 appears to be very weak in the stratum corneum of figure 15b and is not as expected in reference to the theory presented. A study from Garrod et al. 2002 (24) claimed that the desmoglein 1 is normally expressed in the upper layers of the epidermis and this is not observed in figure 15b. A possible explanation could be that the size of desmoglein 1 antibodies used in the experiment was too big and unable to penetrate to the binding sites within the stratum corneum considering that the stratum corneum also acts as a protective barrier.

Cholesteatoma

From figure 12, the “brick and mortar” model as described in the theory for the skin can also be observed in the cholesteatoma STED image. The average width of a single corneocyte in cholesteatoma and the skin was measured and the result is $1.53 \pm 0.27 \mu\text{m}$ and $0.69 \pm 0.16 \mu\text{m}$ respectively (See attachment). The size of the corneocyte in the cholesteatoma are observed to be twice the size of the corneocyte of the skin and does not correlate with the study conducted by Bloksgaard et al. 2012 (2) who claimed that there are no significant difference in the size of corneocyte between the cholesteatoma and the skin. The large black space indicated by the yellow arrow in figure 12 was measured to be $7.17 \mu\text{m}$. A corneocyte of $7.17 \mu\text{m}$ is too big compared to the skin corneocytes and thus leads to the suggestion that the cholesteatoma sample used in figure 12 might have been pulled apart during the slicing process and thus pulling the structures apart by several μm as well.

Cytokeratin 1

Labeling of cytokeratin 1 proteins was successful in the cholesteatoma sample from figure 13a and parallel arrays of keratin filaments as described in the skin stratum corneum can be observed. However, the keratin filaments structures in the cholesteatoma appear unorganized in figure 13a and do not correlates with the observations conducted by Bloksgaard et al. 2012 (2) where it is claimed that the cholesteatoma interior is normally organized as normal human skin stratum corneum. This leads to the suggestion that the structures in the cholesteatoma sample of figure 13a have been disrupted probably during the slicing or labeling process. Figure 7 from the theory section also confirms this suggestion. The figure shows an unsliced sample demonstrating that there are organized structures in the cholesteatoma. This observation thus suggests that the best way to obtain intact structures from the cholesteatoma is to perform experiments on whole cholesteatoma samples instead of sliced samples.

Filaggrin

Labeling of filaggrin proteins was successful in the cholesteatoma sample as seen in figure 14a. Some parallel array patterns were observed in contrast to the intercellular lipids within the montage of figure 14a but unfortunately the labeling is not as expected. To make sure that the labeling is not misinterpreted with autofluorescence already present in the sample, a gray value plot from ImageJ was made and compared to the gray value of the control from figure 9. An intensity ratio between the experiment and the control is 40 to 25. This shows that the intensity of the filaggrin signal from figure 14a is twice that of the intensity of the filaggrin signal from the autofluorescence thus indicating positive labeling of filaggrin in the cholesteatoma sample. The presence of filaggrin in the cholesteatoma indicates that the profilaggrin from the granular layer was dephosphorylated and cleaved forming filaggrin in the cholesteatoma in a similar manner to the filaggrin synthesis in the skin stratum corneum. Figure 14b also support the description mentioned above as a bright filaggrin signal is detected in the lower layer of the stratum corneum. This observation leads to the suggestion that the cholesteatoma stratum corneum behaves and possesses the same properties as the lower zone of the skin stratum corneum.

Referring to the emission spectrum in figure 11, it can be seen that the autofluorescence is greatly reduced above 600 nm. Therefore an improvement that could reduce the presence of autofluorescence from the images would be to use red dye as probe instead of the green dye.

Desmoglein 1

Labeling of desmoglein 1 proteins was successful in the cholesteatoma sample from figure 15a. The desmoglein 1 proteins function as skin cellular spot welds holding adjacent corneocytes together Green et al. 2007 (15) and the desmoglein1 proteins in the cholesteatoma are found as expected together with the intercellular lipids organized similarly to that seen in the skin. Unfortunately in figure 15b, it is not possible to clearly see the desmoglein 1 in the stratum corneum of the skin to compare with the desmoglein 1 structure in figure 15a. Again, considering the intercellular lipids position in figure 15a, the intercellular lipids follow the “brick and mortar” model but appears to be unorganized in contrary to the organized and closely packed structures found in the unsliced cholesteatoma sample from figure 7. This observation suggests that the structures of the cholesteatoma sample might have been disrupted during sample preparation as mentioned previously for the cytokeratin 1 image from figure 13a.

Conclusion

The study has shown that the cholesteatoma resembles the lower layer of the skin stratum corneum. The visible similarity in structures between the cholesteatoma and the skin stratum corneum would also mean similarity in function between the two. The skin is often described as a protective barrier according to literature and as observed in this study, the labeling antibodies could not easily penetrate the stratum corneum giving a poor labeling in the skin stratum corneum images. The labeling of the cholesteatoma by the antibodies on the other hand was visible across the whole sample indicating that the skin is more impermeable than the cholesteatoma. Besides the much larger total thickness of the cholesteatoma stratum corneum in comparison to that of the skin, the thickness of the corneocytes in the cholesteatoma were determined to be twice the thickness of those in the skin suggesting that the corneocytes in the cholesteatoma are not fully matured. This has been observed in corneocytes in inflammatory skin disorders like psoriasis vulgaris and atopic dermatitis where one of the distinguishing features of the diseases is that they consist of immature corneocytes (25). The immature corneocytes and the increased thickness of the cholesteatoma suggests that the barrier in cholesteatoma could be defective, and the defect barrier could then stimulate the increased epidermal proliferation found in the cholesteatoma (3).

Reference

Article reference:

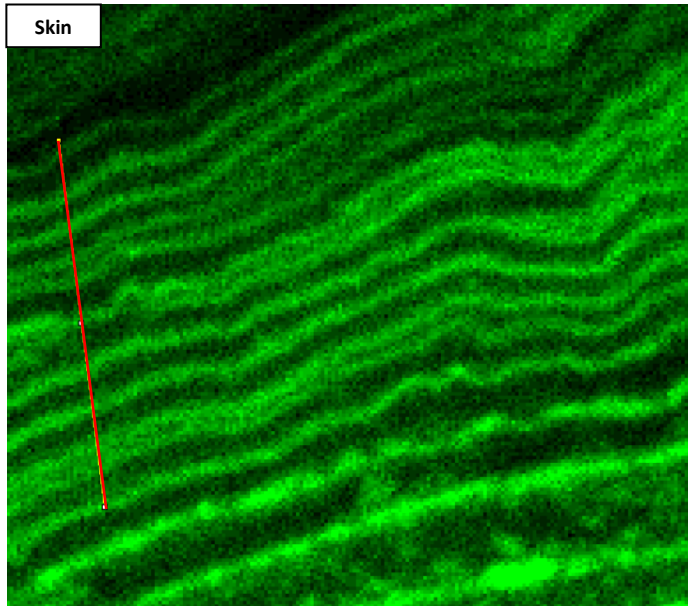
1. Louw L. Acquired cholesteatoma pathogenesis: stepwise explanations. *J Laryngol Otol.* 2010;124(6):587-93.
2. Bloksgaard M, Svane-Knudsen V, Sorensen JA, Bagatolli L, Brewer J. Structural characterization and lipid composition of acquired cholesteatoma: a comparative study with normal skin. *Otol Neurotol.* 2012;33(2):177-83.
3. Proksch E, Feingold KR, Man MQ, Elias PM. Barrier function regulates epidermal DNA synthesis. *J Clin Invest.* 1991;87(5):1668-73.
4. Eckert RL. Structure, function, and differentiation of the keratinocyte. *Physiol Rev.* 1989;69(4):1316-46.
5. Watt FM. Terminal differentiation of epidermal keratinocytes. *Curr Opin Cell Biol.* 1989;1(6):1107-15.
6. Ishida-Yamamoto A, Kishibe M. Involvement of corneodesmosome degradation and lamellar granule transportation in the desquamation process. *Med Mol Morphol.* 2011;44(1):1-6.
7. Matsui T, Amagai M. Dissecting the formation, structure and barrier function of the stratum corneum. *Int Immunol.* 2015.

8. Hennings H, Michael D, Cheng C, Steinert P, Holbrook K, Yuspa SH. Calcium regulation of growth and differentiation of mouse epidermal cells in culture. *Cell*. 1980;19(1):245-54.
9. Menon GK, Cleary GW, Lane ME. The structure and function of the stratum corneum. *Int J Pharm*. 2012;435(1):3-9.
10. Steinert PM, Cantieri JS, Teller DC, Lonsdale-Eccles JD, Dale BA. Characterization of a class of cationic proteins that specifically interact with intermediate filaments. *Proceedings of the National Academy of Sciences of the United States of America*. 1981;78(7):4097-101.
11. Marks R, Plewig G. *Stratum Corneum*. Berlin, Heidelberg: Springer Berlin Heidelberg; 1983.
12. Richter T, Peuckert C, Sattler M, Koenig K, Riemann I, Hintze U, et al. Dead but Highly Dynamic -The Stratum corneum Is Divided into Three Hydration Zones. *Skin pharmacology and physiology*. 2004;17(5):246-57.
13. Kubo A, Ishizaki I, Kubo A, Kawasaki H, Nagao K, Ohashi Y, et al. The stratum corneum comprises three layers with distinct metal-ion barrier properties. *Scientific reports*. 2013;3:1731.
14. Sandilands A, Sutherland C, Irvine AD, McLean WI. Filaggrin in the frontline: role in skin barrier function and disease. *J Cell Sci*. 2009;122(9):1285-94.
15. Green KJ, Simpson CL. Desmosomes: new perspectives on a classic. *The Journal of investigative dermatology*. 2007;127(11):2499-515.
16. Louw L. Acquired cholesteatoma: summary of the cascade of molecular events. *J Laryngol Otol*. 2013;127(6):542-9.
17. Maniu A, Harabagiu O, Perde Schrepler M, Catana A, Fanuta B, Mogoanta CA. Molecular biology of cholesteatoma. *Rom J Morphol Embryol*. 2014;55(1):7-13.
18. Lee RJ, Mackenzie IC, Hall BK, Gantz BJ. The nature of the epithelium in acquired cholesteatoma. *Clin Otolaryngol Allied Sci*. 1991;16(2):168-73.
19. Claxton NS, Fellers TJ, Davidson MW. *Laser Scanning Confocal Microscopy*. 2006.
20. Farahani JN, Schibler MJ, Bentolila LA. Stimulated emission depletion (STED) microscopy: from theory to practice. 2010.
21. Le TT, Yue S, Cheng JX. Shedding new light on lipid biology with coherent anti-Stokes Raman scattering microscopy. *J Lipid Res*. 2010;51(11):3091-102.
22. Potma EO, Xie XS. CARS Microscopy for Biology and Medicine. *Optics and Photonics News*. 2004;15(11):40-5.
23. Manabe M, Sanchez M, Sun TT, Dale BA. Interaction of filaggrin with keratin filaments during advanced stages of normal human epidermal differentiation and in ichthyosis vulgaris. *Differentiation*. 1991;48(1):43-50.
24. Garrod DR, Merritt AJ, Nie Z. Desmosomal cadherins. *Curr Opin Cell Biol*. 2002;14(5):537-45.
25. Hirao T, Terui T, Takeuchi I, Kobayashi H, Okada M, Takahashi M, et al. Ratio of immature cornified envelopes does not correlate with parakeratosis in inflammatory skin disorders. *Experimental dermatology*. 2003;12(5):591-601.

Book reference: Molecular Biology of The Cell, 6th edition, ISBN 978-0-8153-4464-3

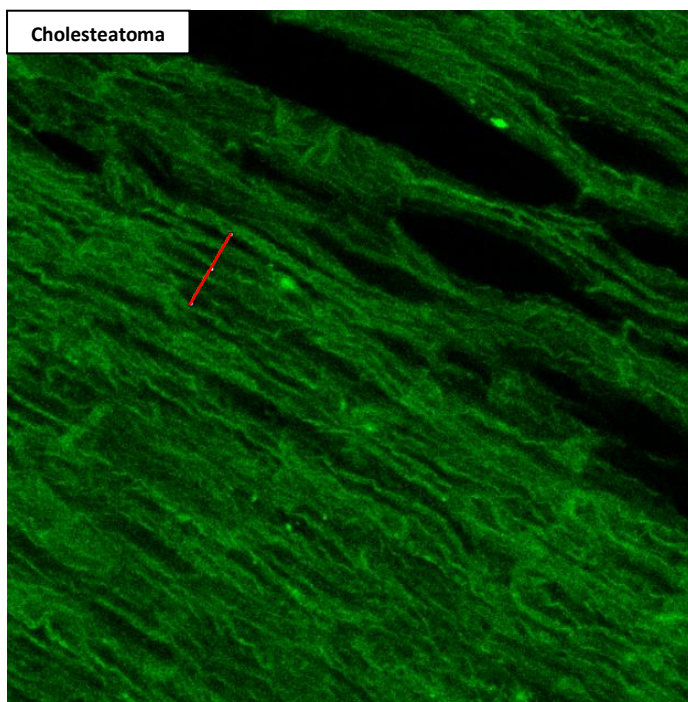
Attachment

The figure and measurements as follows represent the raw data to the width measurements of 10 layers of corneocytes (marked in red by a straight line) from a zoom in skin STED image from figure 12. The standard deviation calculated from the data is ± 0.16 :



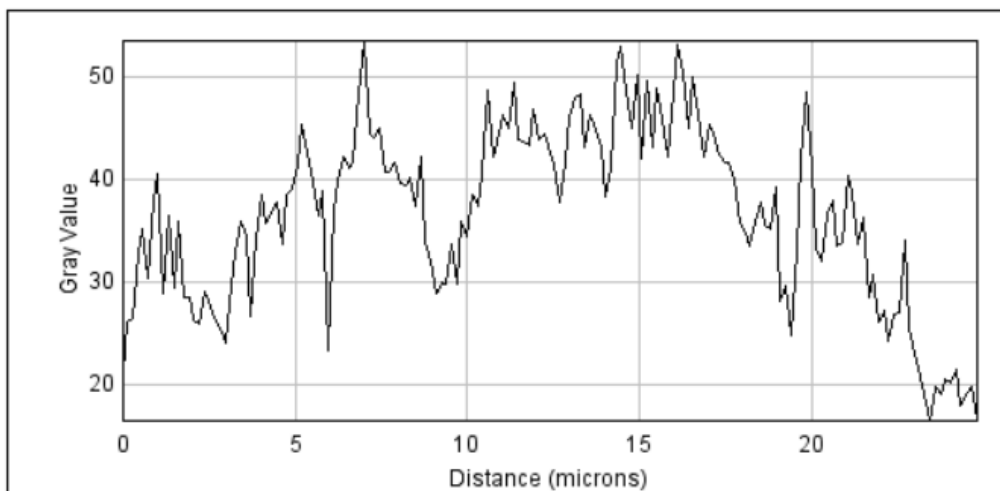
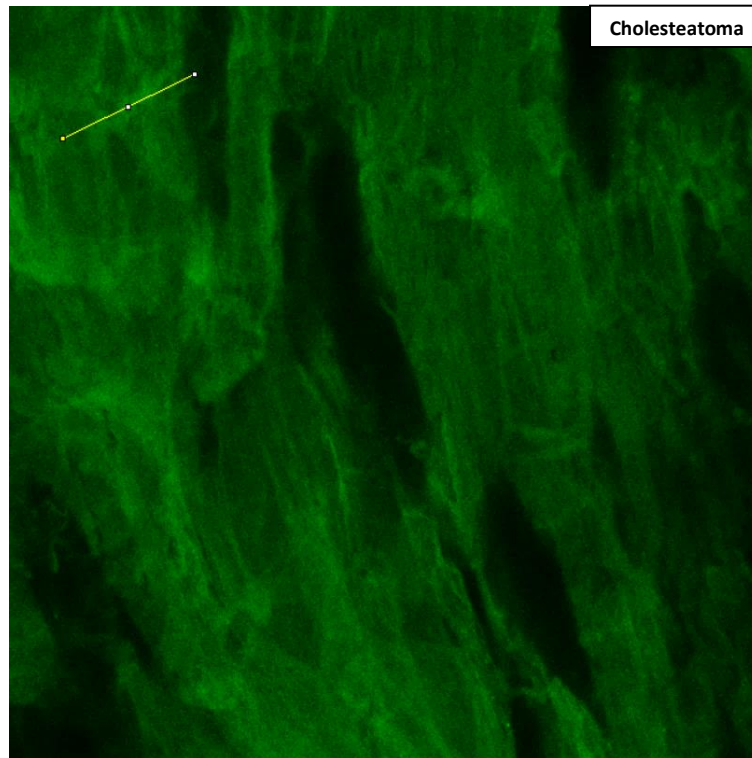
Skin sample	
Layer	Width
1	0.69
2	0.63
3	0.62
4	0.42
5	0.76
6	0.97
7	0.84
8	0.76
9	0.42
10	0.76
Average	0.69±0.16

The figure and measurements as follows are the raw data to the width measurements of 5 layers of corneocytes (marked in red by a straight line) from a zoom in image of the cholesteatoma STED image from figure 12. The standard deviation calculated for the data is ± 0.27 :



Cholesteatoma sample	
Layer	Width
1	1.20
2	1.99
3	1.66
4	1.39
5	1.39
Average	1.53±0.27

The gray value for the filaggrin labeling in the cholesteatoma. The yellow line on the cholesteatoma picture indicates the location where the gray value measurements were performed:



An approximation of 40 is obtained for the gray value of the filaggrin labeling present in the cholesteatoma sample.